Synthesis of Combined Main-Chain/Side-Chain Liquid-Crystalline Polymers via Self-Assembly

Wenyi Huang and Chang Dae Han*

Department of Polymer Engineering, The University of Akron, Akron, Ohio 44325

Received December 20, 2005; Revised Manuscript Received April 24, 2006

ABSTRACT: Three combined main-chain/side-chain liquid-crystalline polymers (MCSCLCPs) were prepared via hydrogen bonding or ionic interactions. The first MCSCLCP, PyHQ12−7CNCOOH, was prepared via hydrogen bonding between the pendent nonmesogenic pyridyl group in a main-chain liquid-crystalline polymer (PyHQ12) and the carboxylic acid group (−COOH) in mesogenic 8-[(4-cyano-4′-biphenyl)oxy]octanoic acid (7CNCOOH). The second MCSCLCP, PABP−AA, was prepared via hydrogen bonding between the nonmesogenic azopyridyl group in the side chain of a main-chain liquid-crystalline polymer (PABP) and the carboxylic acid group (−COOH) in nonmesogenic *p*-anisic acid (AA). The third MCSCLCP, PABP−TSA, was prepared via ionic interactions between the nonmesogenic azopyridyl group in the side chain of PABP and the sulfonic acid group ($-SO_3H$) in nonmesogenic *p*-toluenesulfonic acid (TSA). The presence of hydrogen bonds in self-assembled PyHQ12−7CNCOOH and PABP−AA and the presence of ionic interactions in PABP−TSA were confirmed using Fourier transform infrared (FTIR) spectroscopy, the thermal transitions in each MCSCLCP were determined using differential scanning calorimetry (DSC), and the mesophase structures of each self-assembled MCSCLCP were characterized using polarized optical microscopy (POM) and wide-angle X-ray diffraction (WAXD). The following observations have been made. Self-assembled PyHQ12−7CNCOOH (1) has a nematic mesophase as determined by POM, (2) undergoes a glass transition at ca. 54 °C and nematic-to-isotropic transition at ca. 154 °C as determined by DSC and WAXD, and (3) has a significant degree of hydrogen bonding at temperatures even above its clearing temperature as determined by in situ FTIR spectroscopy. Self-assembled PABP−AA (1) has a smectic mesophase as determined by POM and WAXD, (2) undergoes melting at ca. 120 °C and smectic-to-isotropic transition at ca. 161 °C as determined by DSC, and (3) has a moderate degree of hydrogen bonding at temperatures even above its clearing temperature as determined by in situ FTIR spectroscopy. Self-assembled PABP−TSA (1) has a smectic mesophase as determined by POM, (2) undergoes a glass transition at ca. 58 °C, melting at ca. 110 °C, and smectic-to-isotropic transition at ca. 155 °C as determined by DSC, and (3) has strong ionic interactions as determined by in situ FTIR spectroscopy at temperatures even above the clearing temperature.

1. Introduction

The synthesis of liquid-crystalline polymers (LCPs) has been an active research area for the past three decades. Many of the activities were centered on the syntheses of main-chain liquid-crystalline polymers (MCLCPs)[1−15] and side-chain liquid-crystalline polymers (SCLCPs).[16−28] However, only a relatively small number of research groups[29−38] reported on the synthesis of combined main-chain/side-chain liquid-crystalline polymers (MCSCLCPs). In the synthesis of MCSCLCPs referred to above, two methods have been employed; one method is to attach mesogenic side group(s) onto the flexible methylene units of a semiflexible main-chain polymer,[29−33] and another method is to attach mesogenic side groups as lateral substituents onto the mesogenic moieties of a semiflexible main-chain polymer.[34−38] All the synthesis activities cited above utilized condensation polymerization to synthesize combined MCSCLCPs through covalent bonding.

However, there is another very powerful method to prepare LCPs, namely via self-assembly (e.g., hydrogen bonding). Hydrogen bonding has been discussed extensively in the literature during the past five decades. There are several monographs and hundreds of papers that dealt with hydrogen bonding. The readers are referred to a relatively recent monograph by Jeffrey,[39] who described the fundamental principles involved with hydrogen bonding in general. During the past two decades, several research groups, notably Kato and Fréchet,[40−44] utilized the concept of hydrogen bonding to obtain LCPs. Specifically, in 1989 Kato and Fréchet[40] demonstrated that an LCP can be prepared via hydrogen bonding between a nonmesogenic polymer containing carboxylic acid group and a mesogenic small molecule containing a pyridyl group. In subsequent years, they exploited the concept further to obtain LCPs via hydrogen bonding between a component containing carboxylic acid or acrylic groups and a mesogenic small molecule with a pyridyl group.[41−44] Kato and co-workers[45,46] and Cui and Zhao[47] obtained LCPs via hydrogen bonding between a nonmesogenic polymer containing a pyridine moiety and a compound containing a carboxylic group. Griffith and co-workers[48−50] prepared MCLCPs via hydrogen bonding, and Malik et al.[51] obtained an LCP via hydrogen bonding between two nonmesogenic compounds. The readers are referred to comprehensive review articles by Lehn[52] and Paleos and Tsiourvas,[53] who described the role of intermolecular hydrogen-bonding interactions in the formation of liquid crystals and LCPs.

Very recently, we synthesized two MCSCLCPs via hydrogen bonding. For this, we employed two different methods to obtain self-assembled MCSCLCPs. One method employed was to first synthesize an MCLCP with pendent pyridyl group and then to combine, via hydrogen bonding, with a small mesogenic molecule having a carboxylic acid group in a common solvent, giving rise to a self-assembled MCSCLCP. That is, the formation of a combined MCSCLCP was realized by hydrogen bonding between two mesogenic compounds. Another method employed was to first synthesize an MCLCP having nonmesogenic side chain with azopyridyl group and then to combine,

* To whom correspondence should be addressed. E-mail: cdhan@uakron.edu.

10.1021/ma052716q CCC: $33.50
Published on Web 06/10/2006

Scheme 1. Schematic Describing the Two Methods, (a) Method I and (b) Method II, Employed To Prepare Combined MCSCLCP via Hydrogen Bonding, in Which the Dark Areas Represent Mesogenic Groups

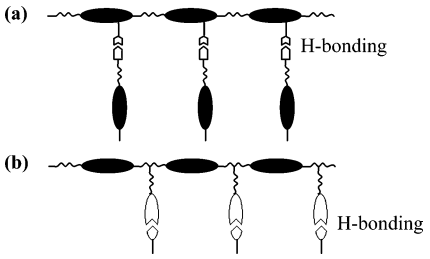

Scheme 2. Synthetic Route for PyHQ12

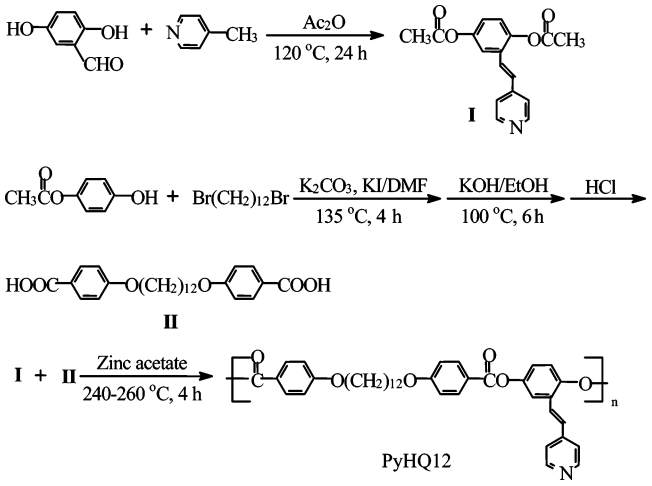

via hydrogen bonding, with a small nonmesogenic molecule having carboxylic acid group in a common solvent, giving rise to a self-assembled MCSCLCP. That is, the formation of a combined MCSCLCP was realized by hydrogen bonding between the nonmesogenic azopyridyl group in the side chain of an MCLCP and a small nonmesogenic molecule having carboxylic acid group, giving rise to a self-assembled MCSCLCP. Using Fourier transform infrared (FTIR) spectroscopy, we confirmed the formation of hydrogen bonds in both MCSCLCPs prepared in this study. The mechanisms through which the two self-assembled MCSCLCPs were prepared in this study are described in Scheme 1.

Earlier, Eisenberg and co-workers[54−56] and Chen et al.[57,58] utilized ionic interactions to enhance the miscibility of immiscible polymer blends. More recently, some investigators[59−61] demonstrated the formation of supramolecular polymers via ionic self-assembly. Very recently, we have prepared a self-assembled MCSCLCP via ionic interactions between the nonmesogenic azopyridyl group in the side chain of an MCLCP and the sulfonic acid group in a small nonmesogenic molecule. We are not aware of any previous study reporting on the formation of self-assembled MCSCLCP via ionic interactions.

In this paper we report the highlights of our findings including the characterization of the three self-assembled MCSCLCPs.

2. Experimental Section

2.1. Synthesis of Self-Assembled PyHQ12−7CNCOOH via Hydrogen Bonding. Self-assembled PyHQ12−7CNCOOH was prepared by first synthesizing an MCLCP having a pyridyl group, PyHQ12, with the reaction route shown in Scheme 2. For the synthesis of PyHQ12, we synthesized the following two monomers: *trans*-2′,5′-diacetoxy-4-stilbazole (**I**) and 4,4′-dicarboxy-1,12-diphenoxydodecane (**II**). In the synthesis of monomer **I**, to a 100 mL flask was added 2,5-dihydroxybenzaldehyde (2.8 g, 20 mmol), 4-picoline (2.4 g, 25 mmol), and 20 mL of acetic anhydride. The reaction mixture was stirred at 120 °C for 24 h. The excessive acetic anhydride and 4-picoline was removed by reduced pressure evaporation. The crude product was then purified using silica gel column chromatography with chloroform/acetone (10/1, v/v) as eluent to give 1.3 g. Yield = 21%; mp = 131 °C. ^{1}H NMR (δ, $CDCl_3$): 2.31 (d, 3H, $-CH_3$), 2.38 (d, 3H, $-CH_3$), 6.99 (d, 1H, −CH−), 7.10 (t, 1H, Ar−H), 7.13 (d, 1H, Ar−H), 7.23 (s, 1H, −CH−), 7.34 (d, 2H, pyridyl−H), 7.42 (d, 1H, Ar−H), 8.59 (d, 2H, pyridyl−H). The synthesis of monomer **II** was conducted by following the method described in the literature.[62] It was obtained in white powder. Yield = 65%; mp = 265 °C. ^{1}H NMR (δ, DMSO) = 1.2−1.45 (m, 16H, $-CH_2-$), 1.69 (m, 4H, $-CH_2-$), 3.99 (t, 4H, $-CH_2O-$), 6.96 (d, 4H, Ar−H), 7.87 (d, 4H, Ar−H). PyHQ12 was obtained via acidolysis by melt polymerization using the following procedures.

To a three-neck 50 mL flask, equipped with an overhead condenser having an argon gas inlet and a vacuum line on the adapter, were added monomer **I** (3.3 g, 10 mmol), monomer **II** (4.4 g, 10 mmol), and 0.02 wt % zinc acetate as catalyst. The reaction mixture was heated to 240 °C in a salt bath, while an argon gas was forced to flow through the reactor. After maintaining the reaction mixture at this temperature for 0.5 h, the temperature was raised to 250 °C and kept there for 3 h, and then a reduced pressure was applied slowly to the system at 260 °C for 0.5 h. A yellowish product was obtained, which was then dissolved in pyridine and precipitated in methanol. The product was filtered and dried in a vacuum oven. Yield = 90%. ^{1}H NMR (δ, pyridine-d_5): 1.2−1.6 (m, 16H, $-CH_2-$), 1.82 (m, 4H, $-CH_2-$), 4.06 (d, 4H, $-CH_2O-$), 6.99 (d, 1H, −CH−), 7.10 (t, 1H, Ar−H), 7.15 (d, 4H, Ar−H), 7.20 (d, 1H, Ar−H), 7.23 (s, 1H, −CH−), 7.36 (d, 2H, pyridyl−H), 7.40 (d, 1H, Ar−H), 7.90 (d, 4H, Ar−H), and 8.60 (d, 2H, pyridyl−H). It should be mentioned that Kato et al.[63] synthesized an LCP similar to PyHQ12, but with 9 methylene flexible spacers in the backbone.

To obtain self-assembled PyHQ12−7CNCOOH, we first synthesized the following mesogenic compound, 8-[(4-cyano-4′-biphenyl)oxy]octanoic acid (hereafter will be referred to as 7CNCOOH), using the reaction procedure described by Lee and Han.[64] Yield = 60%. ^{1}H NMR (δ, DMSO): 1.2−1.55 (m, 6H, $-CH_2-$), 1.70 (m, 4H, $-CH_2-$), 2.19 (t, 2H, $-CH_2-$), 3.99 (t, 2H, $-CH_2O-$), 7.04 (d, 2H, Ar−H), 7.71 (d, 2H, Ar−H), 7.87 (q, 4H, Ar−H), 11.93 (s, 1H, −COOH).

Self-assembled PyHQ12−7CNCOOH was prepared by dissolving equimolar amounts of pyridyl group in PyHQ12 and acid groups in 7CNCOOH in pyridine, yielding a clear solution. Most of the solvent was first evaporated slowly at 60 °C under atmospheric pressure. The remainder of the solution was then dried in a vacuum oven at 100 °C for several days. The mixture formed self-assembled PyHQ12−7CNCOOH via hydrogen bonding between the pyridyl group in PyHQ12 and the carboxylic acid group in 7CNCOOH, as shown below.

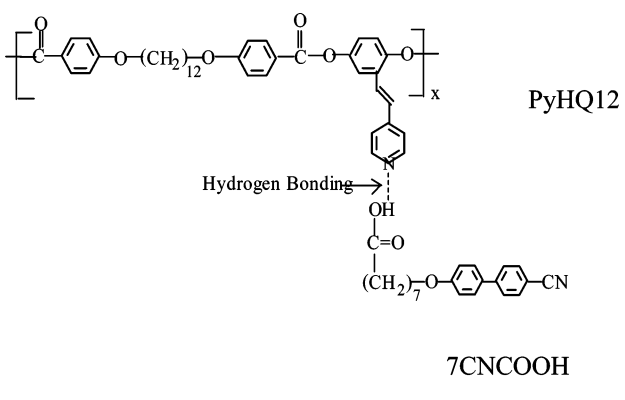

Self-assembled
PyHQ12−7CNCOOH

Scheme 3. Synthetic Route for PABP

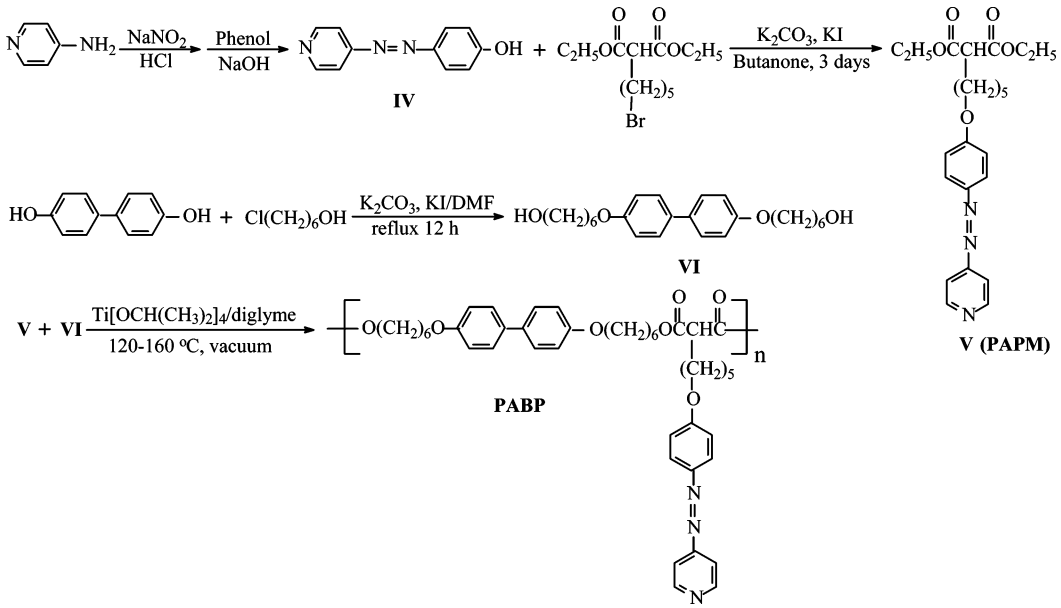

2.2. Synthesis of Self-Assembled PABP-AA via Hydrogen Bonding. Self-assembled PABP-AA was prepared by first synthesizing an MCLCP having azopyridyl side chain, PABP, with the reaction route shown in Scheme 3. For the synthesis of PABP, we synthesized the following three monomers: 4-(4-hydroxyphenylazo)pyridine (**IV**), diethyl 5-[4-(4-pyridylazo)]pentylmalonate (**V**), and 4,4′-bis(6-hydroxy-1-hexyloxy)biphenyl (**VI**).

In the synthesis of monomer **IV**, to a 20 mL of 10% (w/w) NaOH aqueous solution were added phenol (5.0 g, 53 mmol) and sodium nitrate (4.0 g, 58 mmol), which was added dropwise to a solution of 4-aminopyridine (6.0 g, 64 mmol) dissolved in an HCl solution (25 mL of concentrated HCl; 16 mL of distilled water) at 0 °C. After stirring for 30 min, the reaction mixture was adjusted to pH = 6−7 by addition of a 10% (w/w) NaOH aqueous solution. An orange precipitate was collected by filtration. It was then washed with water and dried. Recrystallization from methanol gave 3.5 g of product. Yield = 35%; mp = 265 °C. ^{1}H NMR (δ, DMSO): 6.96 (d, 2H, Ar−H), 7.63 (d, 2H, Ar−H), 7.88 (d, 2H, pyridyl−H), 8.78 (d, 2H, pyridyl-H), 10.56 (s, 1H, −OH).

In the synthesis of monomer **V**, monomer **IV** (2.0 g, 10 mmol) and anhydrous powdered K_2CO_3 (4.1 g, 30 mmol) were dissolved in 30 mL of butanone, and the mixture was stirred at 50 °C for 1 h. Then, a solution of diethyl (5-bromopentyl)malonate dissolved in 20 mL of butanone; a trace of potassium iodide was added to the above mixture, and it was refluxed for 3 days. After filtration and evaporation of the solvent, the crude product was purified using silica gel column chromatography with chloroform/acetone (5/1, v/v) as eluent and then recrystallized from hexane/ethyl acetate (2/1, v/v) to give 3.0 g of orange-colored product. Yield 70%; mp = 66 °C. ^{1}H NMR (δ, $CDCl_3$): 1.28 (t, 6H, $-CH_3$), 1.3−1.55 (m, 4H, $-CH_2-$), 1.78−2.0 (m, 4H, $-CH_2-$), 3.32 (t, 1H, −CH−), 4.06 (t, 2H, $-CH_2O-$), 4.18 (q, 4H, $-CH_2COO-$), 7.01 (d, 2H, Ar−H), 7.75 (d, 2H, Ar−H), 7.96 (d, 2H, pyridyl−H), 8.78 (d, 2H, pyridyl−H).

In the synthesis of monomer **VI**, 4,4′-bis(6-hydroxy)biphenyl (2.9 g, 15 mmol) was added to a solution of K_2CO_3 (20.7 g, 150 mmol) in 100 mL of DMF. After the addition of 6-chloro-1-hexanol (6.4 g, 45 mmol) and a trace of potassium iodide, the mixture was refluxed for 12 h and then neutralized with HCl and diluted with 200 mL of distilled water. The precipitate was recrystallized from chloroform to give 2.8 g of white solid. Yield = 50%. ^{1}H NMR (δ, DMSO): 1.25−1.50 (m, 12H, $-CH_2-$), 1.70 (m, 4H, $-CH_2-$), 3.38 (q, 4H, $-CH_2-$), 3.96 (t, 4H, $-CH_2O-$), 4.30 (t, 2H, −OH), 6.95 (d, 4H, Ar−H), 7.46 (d, 4H, Ar−H).

PABP was obtained via transesterification by melt polymerization using the following procedures. To a three-neck 50 mL flask, equipped with an overhead condenser with argon gas inlet and vacuum line on the adapter, were added monomer **V** (2.14 g, 5 mmol) and monomer **VI** (1.93 g, 5 mmol). The mixture was molten and stirred at 120 °C under argon gas flow. After the addition of titanium isoproxide (12.3 mg in 120 μL of diethylene glycol dimethyl ether), bubbles of ethanol became visible. Upon stirring for 15 min, a low vacuum was applied for 15 min. Thereafter, an oil pump was used. The temperature was raised to 160 °C for 10 h. Afterward, the polymer was purified by dissolution in chloroform and precipitated in acetone. Yield = 92%. ^{1}H NMR (δ, $CDCl_3$): 1.25−1.5 (m, 16 H, $-CH_2-$), 1.55−1.9 (m, 8H, $-CH_2-$), 3.28 (t, 1H, −CH−), 3.88 (t, 4H, $-CH_2O-$), 3.95 (t, 2H, $-CH_2O-$), 4.06 (t, 4H, $-CH_2O-$), 6.82 (d, 4H, Ar−H), 6.95 (d, 2H, Ar−H), 7.34 (d, 4H, Ar−H), 7.58 (d, 2H, Ar−H), 7.85 (d, 2H, pyridyl−H), 8.68 (d, 2H, pyridyl−H).

Self-assembled PABP−AA was prepared by dissolving equimolar amounts of azopyridyl group in PABP and carboxylic acid group in *p*-anisic acid (AA) in chloroform, yielding a clear solution (heated slightly to 50 °C to ensure complete solubilization). Most of the solvent was first evaporated slowly under atmospheric pressure. The remainder of the solution was then dried in a vacuum at 100 °C for several days. The mixture formed self-assembled PABP−AA via hydrogen bonding between the pyridyl group in the nonmesogenic azopyridine side chain and the carboxylic acid group in AA, as shown below.

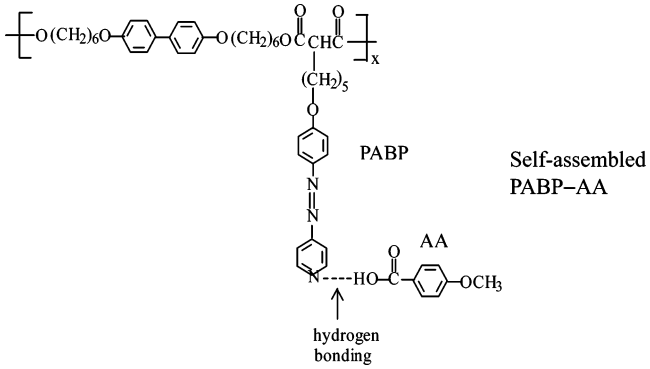

2.3. Preparation of Self-Assembled PABP−TSA via Ionic Interactions. Self-assembled PABP−TSA was prepared by dissolving equimolar amounts of azopyridyl group in PABP and sulfonic acid group in *p*-toluenesulfonic acid (TSA) in chloroform, yielding a clear solution (heated slightly to 50 °C to ensure complete

solubilization). Most of the solvent was first evaporated slowly under atmospheric pressure. The remainder of the solution was then dried under vacuum at 100 °C for several days. The mixture formed self-assembled PABP−TSA via ionic interactions between the pyridyl group in the nonmesogenic azopyridine side chain and the sulfonic acid group in TSA, as shown below.

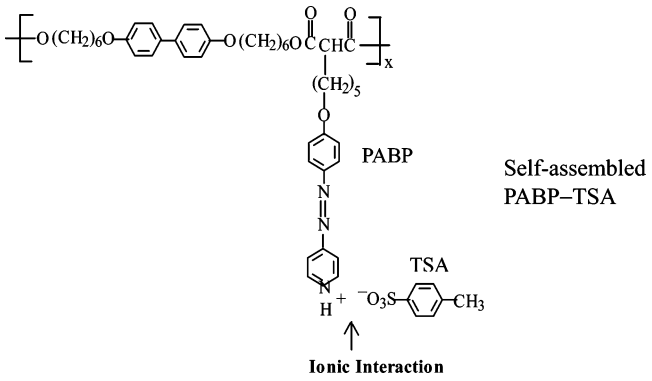

2.4. Experimental Methods Employed for the Characterization of the Polymers Synthesized. (a) Nuclear Magnetic Resonance (NMR) Spectroscopy. Using NMR spectroscopy, we identified the chemical structures of the various compounds synthesized. NMR spectra were obtained with a Varian Gemini 300 MHz NMR spectrometer. Deuterated dimethyl sulfoxide (DMSO-d_6), chloroform ($CDCl_3$-d), and pyridine-d_5 were used as solvents.

(b) Differential Scanning Calorimetry (DSC). Using DSC, we determined the thermal transition temperatures of the various compounds synthesized. DSC thermograms were obtained with a Perkin-Elmer DSC-7 differential scanning calorimeter, using indium as the calibration standard and a heating or cooling rate of 20 °C/min under a nitrogen atmosphere. The glass transition temperature (T_g) was determined as the midpoint of the step change in the heat capacity, while the melting and clearing temperatures were determined from the maximum of the endothermic peak. All DSC runs were made under a nitrogen atmosphere with heating and/or cooling rates of 20 °C/min.

(c) Wide-Angle X-ray Diffraction (WAXD). Room temperature WAXD experiments were conducted on the as-cast films and melt-drawn fibers of both neat polymers and self-assembled MCSCLCPs, using a General Electric X-ray generator (model XRD-6) operated at 30 kV and 30 mA (Ni-filtered Cu K_α radiation). The flat-plate diffraction patterns were recorded with a 53.3 mm film-to-specimen distance. The exposure time for each measurement was 4 h. Also conducted were variable-temperature WAXD experiments on as-cast films of PABP and self-assembled MCSCLCPs during heating and cooling cycles by Prof. Jin Kon Kim at Pohang University of Science and Technology in the Republic of Korea. For the experiments, an 18 kW Rigaku rotating-anode X-ray generator operated at 46 kV and 20 mA, mirror optics having point focusing, and one-dimensional position sensitive detector (M. Braun) were employed. The Cu K_α radiation from a 0.1 × 1 mm microfocus cathode was used. The thickness of the sample was 1 mm, and the distance between the sample and the detector was 10.5 cm. Variable-temperature WAXD experiments were conducted at 150, 140, 130, 120, 110, and 100 °C in the first cooling cycle and at 25, 60, 90, 100, 110, 120, 130, 140, 150, and 160 °C in the second heating cycle.

(d) X-ray Diffraction (XRD). Using a Rigaku X-ray generator operated at 40 kV and 150 mA, X-ray diffraction patterns were obtained to determine the mesophase and crystalline structures of self-assembled MCSCLCPs. The X-ray beam was monochromatized to Cu K_α with a graphite crystal. The range of 2θ scanning of X-ray intensity employed was 1.5°−35°.

(e) Fourier Transform Infrared (FTIR) Spectroscopy. Using a Fourier transform infrared spectrometer (16 PC FTIR, Perkin-Elmer), in situ FTIR spectra were obtained at temperatures ranging from 25 to 170 °C for self-assembled PyHQ12−7CNCOOH, self-assembled PABP−AA, and PABP−TSA. The temperature was measured at the sample surface and controlled to within ±1.0 °C using a proportional-integral-derivative controller. Specimens were maintained at a preset temperature for 5 min prior to data acquisition. FTIR spectra for other specimens were obtained at room temperature. Spectral resolution was maintained at 4 cm^{-1}. Dry nitrogen gas was used to purge the sample compartment to reduce the interference of water and carbon dioxide in the spectrum. Thin films suitable for FTIR spectroscopy were prepared by casting 2% (w/v) solution in pyridine directly on the KBr salt plate. Film thickness was adjusted, such that the maximum absorbance of any band was less than 1.0, at which the Beer−Lambert law is valid. Film specimens were slowly dried for 24 h in a fume hood until most of the solvent evaporated and then dried at 80 °C for a few days in a vacuum oven, and they were then stored in a vacuum oven until use.

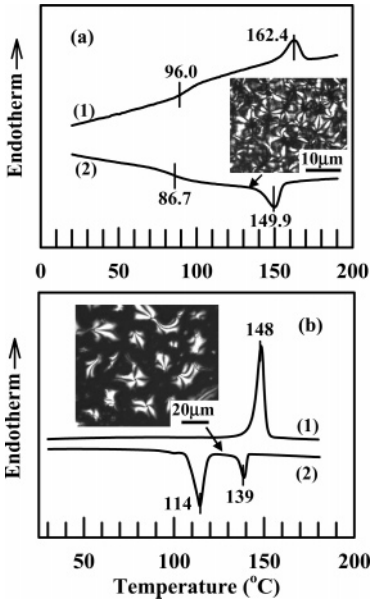

Figure 1. DSC thermograms for (a) PyHQ12 and (b) 7CNCOOH at a scanning rate of 20 °C/min during (1) heating and (2) cooling cycles and their POM images at 130 °C during the cooling cycle.

(f) Polarized Optical Microscopy (POM). The mesophase structures of the liquid-crystalline phase of PyHQ12, self-assembled PyHQ12−7CNCOOH, PABP, self-assembled PABP-AA, and self-assembled PABP-TSA were investigated, via POM, using a Leitz Laborlux 12 Pol S polarized optical microscope equipped with a hot stage (Instec) and a digital camera (Spot insight 2, Diagnostic Instrument). Specimens were cast from 1 wt % solution of neat polymer or self-assembled MCSCLCP on a slide glass to obtain a film of about 2−3 μm in thickness, which was initially dried in a fume hood and then in a vacuum oven. The heating and cooling rates employed were 3 °C/min. Images of POM were obtained after keeping a specimen at a preset temperature for at least 10 min.

3. Results and Discussion

3.1. Self-Assembled PyHQ12−7CNCOOH via Hydrogen Bonding. (a) Thermal Transition and Mesophase Structure of Self-Assembled PyHQ12−7CNCOOH. Figure 1 gives DSC thermograms for (a) PyHQ12 and (b) 7CNCOOH at a scanning rate of 20 °C/min during heating and cooling cycles. The following observations are worth noting in Figure 1. (i) PyHQ12 has a T_g of 96 °C and a clearing temperature of 162 °C during heating. The POM image given in the inset of Figure 1a indicates that PyHQ12 has Schlieren texture (thus nematic mesophase) at temperatures between 96 and 162 °C, and thus 162 °C represents the nematic-to-isotropic (N−I) transition temperature (T_{NI}). (ii) Referring to Figure 1b, during heating

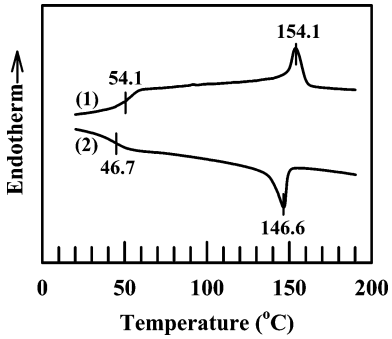

Figure 2. DSC thermograms for self-assembled PyHQ12−7CNCOOH at a scanning rate of 20 °C/min during (1) heating and (2) cooling cycles.

the mesogenic small molecule 7CNCOOH has a T_{NI} of 148 °C, while during cooling it undergoes two thermal transitions: (1) isotropic-to-nematic (I−N) transition at 139 °C, which is 9 °C lower, owing to supercooling, than the T_{NI} determined during heating and (2) crystallization at 114 °C. The POM image shown in Figure 1b indicates that 7CNCOOH has Schlieren texture (thus nematic mesophase) upon cooling.

Figure 2 gives DSC thermograms for self-assembled PyHQ12−7CNCOOH during the heating and cooling cycles at a scanning rate of 20 °C/min. It is seen in Figure 2 that during heating PyHQ12−7CNCOOH undergoes a glass transition at ca. 54 °C and N−I transition at ca. 154 °C, and both T_g and T_{NI} during cooling are slightly lower, owing to supercooling, than those during heating. Comparison of Figure 2 with Figure 1a indicates that the T_g of self-assembled PyHQ12−7CNCOOH is ca. 42 °C lower than that of PyHQ12, and the T_{NI} of self-assembled PyHQ12−7CNCOOH is ca. 8 °C lower than that of PyHQ12. Also, there is no evidence of crystallization in PyHQ12−7CNCOOH during cooling. The observed decrease in T_g of self-assembled PyHQ12−7CNCOOH is attributable to the attachment of side-chain mesogenic 7CNCOOH onto the backbone of PyHQ12 via hydrogen bonding between the pendent pyridyl group in PyHQ12 and the carboxylic acid group in 7CNCOOH.

It is worth pointing out that the observed decrease in T_g and T_{NI} of PyHQ12 in the mixtures of PyHQ12 and 7CNCOOH could not have occurred if 7CNCOOH did not bind to PyHQ12 and instead acted as a nematic solvent. Note that 7CNCOOH melts at 148 °C during heating (see DSC thermograms in Figure 1b), and thus it cannot act as a nematic solvent at temperatures below 148 °C. If 7CNCOOH did not bind to PyHQ12 and acted as a nematic solvent, during cooling 7CNCOOH in the mixture with PyHQ12 should have undergone crystallization at 114 °C (see DSC thermograms in Figure 1b). However, the DSC thermograms of the mixture of PyHQ12 and 7CNCOOH exhibit only a single exothermic peak at 146 °C during cooling (see Figure 2); i.e., there is no evidence that crystallization of 7CNCOOH took place during cooling in the mixture of PyHQ12 and 7CNCOOH. The above observations indicate clearly that 7CNCOOH did not act as a nematic solvent; rather, it was bound to PyHQ12 forming self-assembled PyHQ12−7CNCOOH.

We obtained DSC thermograms for PyHQ12−7CNCOOH specimens, although not presented here, after they were annealed from 6 to 48 h, indicating that annealing up to 48 h has a relatively small effect on the T_g and T_{NI} of PyHQ12−7CNCOOH. Further, annealing for a long period did not produce a new endothermic peak. These observations indicate that self-assembled PyHQ12−7CNCOOH via hydrogen bonding is thermally stable and little affected by isothermal annealing for an extended period.

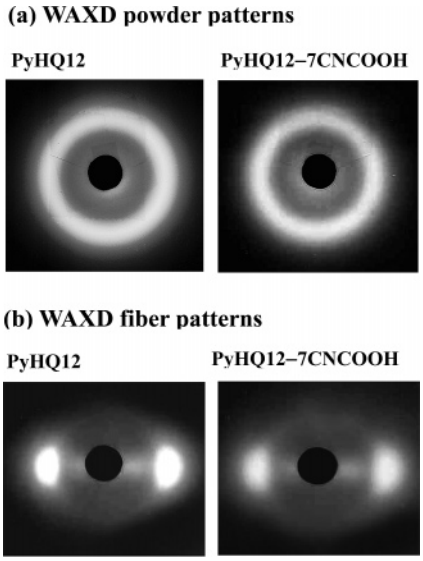

Figure 3. (a) WAXD powder patterns of PyHQ12 and self-assembled PyHQ12−7CNCOOH after annealing at 130 °C for 48 h. (b) WAXD fiber patterns of unannealed melt-drawn specimens of PyHQ12 and self-assembled PyHQ12−7CNCOOH.

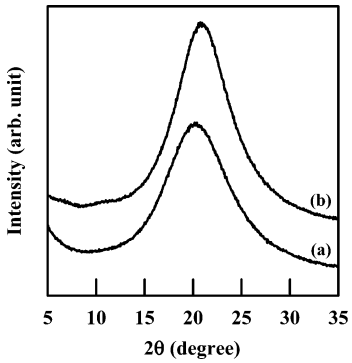

Figure 4. XRD patterns of (a) PyHQ12 and (b) self-assembled PyHQ12−7CNCOOH at room temperature.

(b) WAXD and XRD Patterns of PyHQ12 and Self-Assembled PyHQ12−7CNCOOH. Figure 3a gives WAXD powder patterns for PyHQ12 and PyHQ12−7CNCOOH, indicating that even after annealing at 130 °C for 48 h both PyHQ12 and PyHQ12−7CNCOOH still have very diffuse diffraction in powder patterns, and no crystalline structures are discernible. In the WAXD fiber patterns given in Figure 3b, both PyHQ12 and PyHQ12−7CNCOOH have only diffuse lateral spacings. Figure 4 gives XRD patterns for PyHQ12 and self-assembled PyHQ12−7CNCOOH, showing that they only exhibit strong peaks at 2θ of 21°, confirming the observations made in Figure 3 for WAXD patterns. On the basis of the DSC thermograms (Figures 1a and 2) and the WAXD patterns presented in Figure 3, we conclude that both PyHQ12 and self-assembled PyHQ12−7CNCOOH are glassy nematic polymers.

(c) POM Images of Self-Assembled PyHQ12−7CNCOOH. Figure 5 gives POM images of self-assembled PyHQ12−7CNCOOH during heating from 120 to 160 °C and during cooling from the isotropic state to 25 °C. The significance of Figure 5 lies in that, interestingly, upon cooling from the isotropic state the nematic structure appears very rapidly in the self-assembled PyHQ12−7CNCOOH. It should be mentioned that phase separation in PyHQ12−7CNCOOH did not occur even when a specimen was raised to a temperature well above its T_{NI} (ca. 154 °C), suggesting that little breakdown of the hydrogen bonds formed between the pyridyl group and car-

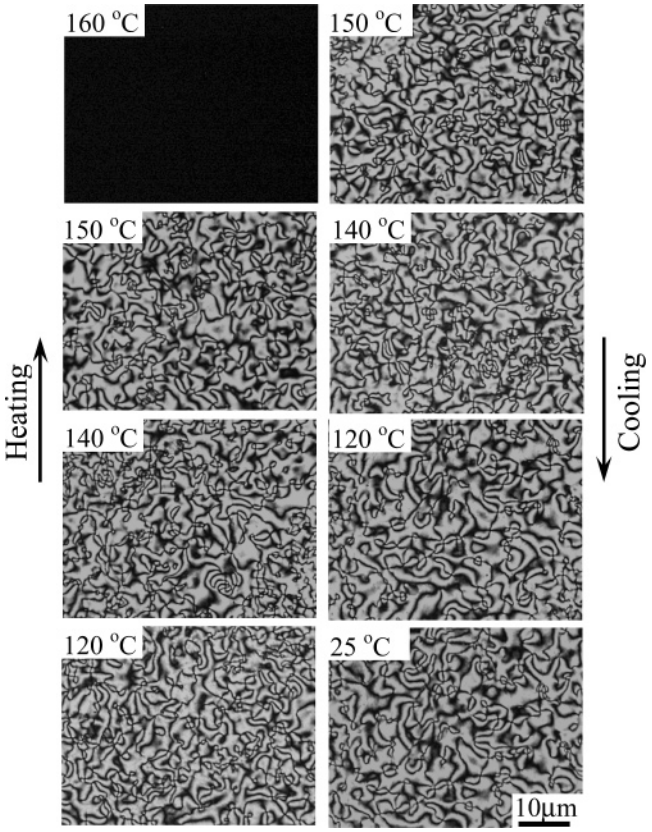

Figure 5. POM images of self-assembled PyHQ12−7CNCOOH upon heating from 120 to 160 °C (above the T_{NI} = 154.1 °C) and during cooling from the isotropic state to 25 °C.

boxylic acid group appeared to have taken place. What surprised us during our in situ POM experiments was that the reappearance of nematic mesophase, upon cooling from the isotropic state, was very rapid. Later, we learned the reason for the unexpected experimental observation from conducting in situ FTIR experiments.

(d) FTIR Spectra of Self-Assembled PyHQ12−7CNCOOH. Figure 6a gives FTIR spectra for 7CNCOOH, and Figure 6b gives FTIR spectra for PyHQ12 at room temperature (denoted by *) and in situ FTIR spectra for self-assembled PyHQ12−7CNCOOH, during heating, at various temperatures ranging from 25 to 170 °C. The following observations are worth noting in Figure 6. (i) Two absorption peaks appear at wavenumbers of 2500 and 1930 cm^{-1} for self-assembled PyHQ12−7CNCOOH, in contrast to the FTIR spectra for 7CNCOOH and PyHQ12. According to the literature,[63] hydrogen-bonded and Fermi resonance absorption peaks are expected to appear at those two wavenumbers when hydrogen-bonded complexes are formed between pyridine and carboxylic acid derivatives. (ii) As the temperature is increased, the absorption peaks at wavenumbers of 2500 and 1930 cm^{-1} persist even at 170 °C, which is well above the T_{NI} (ca. 154 °C) of PyHQ12−7CNCOOH, although the strength of the absorption peak at a wavenumber of 2500 cm^{-1} is weakened slightly. (iii) The disappearance of a typical absorption peak at a wavenumber of 1704 cm^{-1} for the carboxylic acid (hydrogen-bonded dimer) in 7CNCOOH is attributable to a shifting to a higher absorption peak due to the formation of hydrogen bonds with the pyridyl groups in PyHQ12, thus overlapping with the absorption peak at a wavenumber of 1732 cm^{-1} for the carbonyl groups in PyHQ12. According to the literature,[65] the strength of hydrogen bonds between the phenolic hydroxyl group and the acetate carbonyl group in a polymer blend decreases with increasing

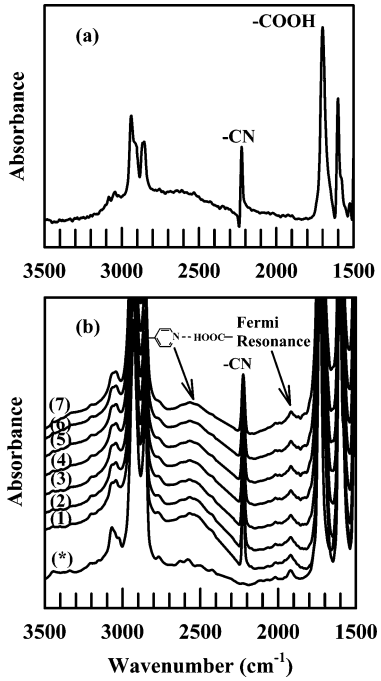

Figure 6. FTIR spectra for (a) 7CNCOOH and (b) PyHQ12 denoted by (*) at room temperature and in situ FTIR spectra for self-assembled PyHQ12−7CNCOOH at various temperatures (°C): (1) 25, (2) 100, (3) 120, (4) 140, (5) 150, (6) 160, and (7) 170.

temperature. However, in Figure 6b we observe that the attractive interactions between the pendent pyridyl group in PyHQ12 and the carboxylic group in 7CNCOOH in self-assembled PyHQ12−7CNCOOH are strong enough to persist over the entire range of temperatures investigated. This seems to suggest that the attractive interactions between the pyridyl group and carboxyl acid group are much stronger than those between the phenolic hydroxyl group and acetate carbonyl group. Notice in Figure 5 that we observe a complete disappearance of nematic mesophase in self-assembled PyHQ12−7CNCOOH at 160 °C, which is ca. 6 °C above its T_{NI}. Yet, in Figure 6b we observe that a significant degree (strength) of hydrogen bonding still persists at 160 and 170 °C. This observation now explains why we observed, during cooling from the isotropic region, a very rapid reappearance of nematic mesophase in PyHQ12−7CNCOOH upon passing the isotropic-to-nematic (I−N) transition temperature (T_{IN}).

3.2. Self-Assembled PABP-AA via Hydrogen Bonding. (a) Formation of Hydrogen Bonds Between Monomer PAPM and *p*-Anisic Acid. In this study we had to first confirm that PABP is an MCLCP, i.e., the azopyridyl group in the side chain of PABP is nonmesogenic, and then ascertain that the azopyridyl group in monomer PAPM (monomer **V** designated in Scheme 3), when it is mixed with *p*-anisic acid (AA), forms a mesogenic phase. These two steps were necessary for us to conclude that self-assembled PABP-AA is indeed a combined MCSCLCP. Figure 7a gives DSC thermograms for PAPM at a scanning rate of 20 °C/min, showing only a melting temperature of 66.4 °C during heating, while it undergoes crystallization, during cooling, at 19.6 °C. The POM image (not presented here) has assured us that no mesophase exists in PAPM and that a crystalline structure forms, during cooling, at temperatures below 20 °C. Thus, we have concluded that PAPM does not exhibit liquid-crystalline characteristics (i.e., PAPM is a nonmesogenic compound and thus PABP having azopyridyl side chain is an MCLCP). Next, we prepared a mixture of PAPM and AA in a common solvent (acetone) and then slowly evaporated the

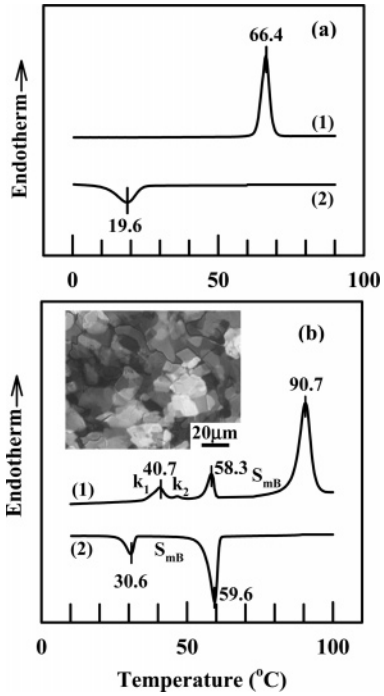

Figure 7. DSC thermograms for (a) PAPM (in which 66.4 °C denotes melting temperature) and (b) self-assembled PAPM−AA at a scanning rate of 20 °C/min during (1) heating and (2) cooling cycles and POM image taken at 50 °C during the cooling cycle. Here k denotes the crystalline state, and SmB denotes the smectic B phase.

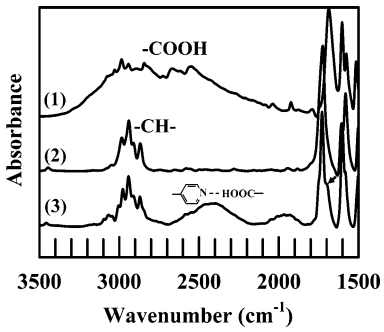

Figure 8. FTIR spectra for (1) AA, (2) PAPM, and (3) self-assembled PAPM−AA at room temperature.

solvent followed by drying in a vacuum oven at 60 °C. Figure 7b gives DSC thermograms for a mixture of PAPM and AA at a scanning rate of 20 °C/min. It can be seen that during heating the mixture undergoes a crystal-to-crystal (k1−k2) transition at 40.7 °C, then a crystal-to-smectic (k2−S) transition at 58.3 °C, and finally smectic-to-isotropic (S−I) transition at 90.7 °C, while during cooling the mixture undergoes an isotropic-to-smectic (I−S) transition at ca. 60 °C followed by a smectic-to-crystal transition (S−k2) at ca. 31 °C. In the inset of Figure 7b is given a POM image, taken at 50 °C during cooling, for a mixture of PAPM and AA, confirming the presence of a mosaic mesophase structure (smectic B). Thus, we have concluded that a mixture of PAPM and AA has induced a mesogenic phase via hydrogen bonding between the azopyridine group in PAPM and the carboxylic acid group in AA.

Figure 8 gives FTIR spectra for (1) *p*-anisic acid, (2) PAPM, and (3) self-assembled PAPM−AA at room temperature. It can be seen in Figure 8 that self-assembled PAPM−AA has two new absorption bands: one absorption peak at a wavenumber of 2500 cm^{-1} representing hydrogen-bonded carboxylic acid with a pyridyl group and another absorption peak at a wavenumber of 1940 cm^{-1} representing a Fermi resonance. The

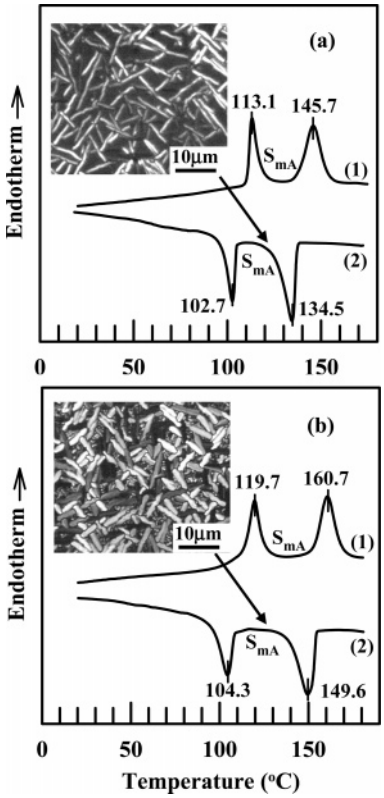

Figure 9. DSC thermograms for (a) PABP and (b) self-assembled PABP−AA at a scanning rate of 20 °C/min during (1) heating and (2) cooling cycles and their POM images taken at 130 °C during the cooling cycle.

absorption peak at a wavenumber of 1680 cm^{-1} characteristic of carboxylic acid (stretching of −OH group) is shifted to a higher wavenumber (ca. 1710 cm^{-1}), close to that of the carbonyl group of PAPM (a shoulder shown in spectrum (3) in Figure 8). Also, the absorption peak for azopyridine at a wavenumber of 1596 cm^{-1} is shifted to 1604 cm^{-1}, overlapped by the absorption peak of benzene ring of *p*-anisic acid. The above observations have ensured us that the azopyridyl group in monomer PAPM, when it was mixed with *p*-anisic acid (AA), indeed formed a mesogenic phase.

(b) Thermal Transition and Mesophase Structures of PABP and Self-Assembled PABP-AA. Figure 9 gives the DSC thermograms for PABP and self-assembled PABP-AA during the heating and cooling cycles at a scanning rate of 20 °C/min. In the insets of Figure 9a,b are given POM images, taken at 130 °C, of PABP and self-assembled PABP-AA, showing that both have needle-type (batonnet texture) smectic A mesophase. It can be seen in Figure 9a that during heating PABP has a melting temperature (T_m) of ca. 113 °C and a smectic-to-isotropic (S−I) transition temperature (T_{SI}) of ca. 146 °C, while during cooling its crystallization temperature and isotropic-to-smectic (I−S) transition temperature (T_{IS}) are slightly lower than the melting and clearing temperatures observed during heating. Notice in Figure 9b that self-assembled PABP-AA has a T_m of ca. 120 °C and a T_{SI} of ca. 161 °C, which are slightly higher than those of PABP. An increase of T_{SI} of self-assembled PABP-AA by 15 °C over that of PABP is attributed to the formation of hydrogen bonds between the azopyridyl group in the side chain of PABP and the carboxylic acid group in *p*-anisic acid, giving rise to a mesogenic side chain.

(c) WAXD and XRD Patterns of PABP and Self-Assembled PABP-AA. Figure 10 gives WAXD powder patterns of (a) PABP and (b) self-assembled PABP-AA. It is seen in

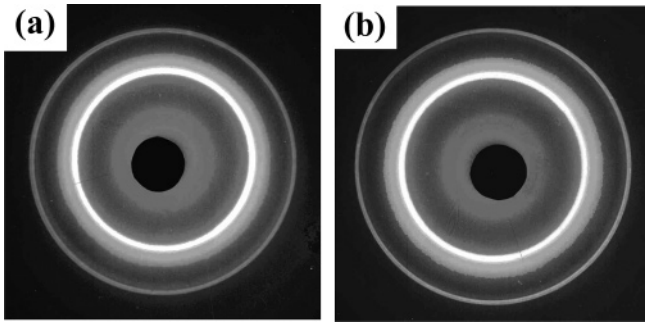

Figure 10. WAXD powder patterns of (a) PABP and (b) self-assembled PABP−AA at room temperature.

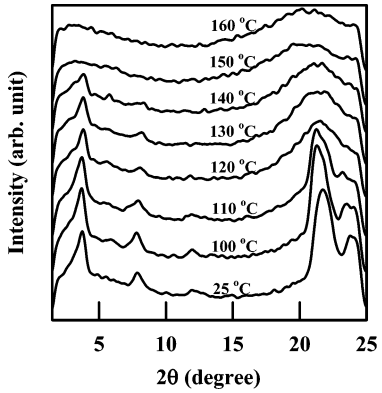

Figure 11. Variation of the X-ray diffraction intensity with scattering angle 2θ for an as-cast PABP during the second heating cycle at various temperatures, as indicated in the plot.

Figure 10 that both PABP and self-assembled PABP-AA exhibit remarkably similar X-ray diffraction patterns, indicating that the attachment of a small nonmesogenic molecule, *p*-anisic acid, to PABP has changed little the mesophase structure of PABP. This observation confirms the POM images of PABP and self-assembled PABP-AA, both forming smectic-A mesophase at temperatures between T_m and T_{SI}, given in the insets of Figure 9a,b.

Figure 11 gives variations of XRD intensity for PABP with scattering angle 2θ for an as-cast PABP specimen during the second heating cycle at various temperatures, as indicated on the plot. The following observations are worth noting in Figure 11. (1) Below the melting temperature (T_m = ca. 113 °C) of PABP, there are two reflection peaks, at 2θ = ca. 12° (d = 7.37 Å) and at 2θ = ca. 23.5° (d = 3.78 Å), which are assigned to the crystalline structure of PABP because these two peaks disappear as the temperature is increased above T_m. (2) Below the clearing temperature (T_{SI} = ca. 145 °C), the strongest peak appears at 2θ = 21.8° (d = 4.08 Å), which corresponds to the very strong bright ring in the WAXD powder patterns given in Figure 10a and is due to the distance between the planes on which the oriented mesogenic groups lies. There are two additional small reflection peaks, at 2θ = ca. 3.7° (d = 23.85 Å) and at 2θ = ca. 7.8° (d = 11.32 Å), suggesting the presence of smectic A mesophase, and they persist until the temperature is raised above T_{SI}. Previously, similar XRD patterns were reported on other LCPs forming smectic A mesophase.[66,67] (3) When the temperature is increased to T_{SI}, all peaks disappear, except for a broad peak at 2θ = ca. 20°, confirming the presence of an isotropic melt. In the present study, we also obtained variable-temperature XRD intensities of self-assembled PABP−AA, which look virtually identical to those shown in Figure 11. This is not surprising in that we already have shown that POM images (Figure 9) and WAXD powder patterns

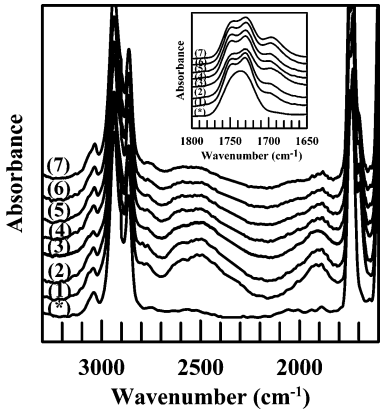

Figure 12. FTIR spectrum for PABP denoted by (*) and in situ FTIR spectra for self-assembled PABP-AA at various temperatures (°C): (1) 25, (2) 100, (3) 120, (4) 140, (5) 150, (6) 160, and (7) 170. The inset shows the absorption peaks at wavenumbers ranging from 1800 to 1650 cm^{-1}.

(Figure 10) of self-assembled PABP-AA are virtually the same as those of PABP. Thus, we have chosen not to present here the variable-temperature XRD intensities of self-assembled PABP−AA. Therefore, we conclude that both PABP and self-assembled PABP−AA are semicrystalline, smectic-forming liquid-crystalline polymers.

(d) In Situ FTIR Spectra for Self-Assembled PABP-AA. Figure 12 gives FTIR spectrum for PABP taken at room temperature (denoted by *), and in situ FTIR spectra for self-assembled PABP-AA at various temperatures, during heating, ranging from 25 to 170 °C. The following observations are worth noting in Figure 12. (1) Two absorption peaks appear at wavenumbers of 2500 and 1900 cm^{-1} in self-assembled PABP-AA, in contrast to the spectra for PABP and AA. It is clearly seen in Figure 12 that the attractive interactions between the azopyridyl group in the side chain of PABP and the carboxylic acid group in AA are much stronger than the self-association within PABP molecules. (2) As the temperature is increased, the absorption peaks at wavenumbers of 2500 and 1900 cm^{-1} for PABP−AA persist even at 170 °C, which is above its T_{SI} (161 °C), although the strength of the absorption peak at a wavenumber of 2500 cm^{-1} is somewhat weakened. (3) From the inset of Figure 12 we observe that the absorption peak at a wavenumber of 1680 cm^{-1} for the carboxylic acid group in anisic acid (see spectrum (1) in Figure 8) has become a shoulder, getting stronger as the temperature is increased, while the absorption peak at a wavenumber of 1732 cm^{-1} for carbonyl group of PABP becomes broader and a new stronger peak appears at a wavenumber of 1726 cm^{-1}, which has originated from the formation of hydrogen bonds between the azopyridyl group in the side chain of PABP and the carboxylic acid group in AA.

3.3. Self-Assembled PABP-TSA via Ionic Interactions. (a) Formation of a Mesogenic Phase in a Mixture of Monomer PAPM and *p*-Toluenesulfonic Acid via Ionic Interactions. In Figure 7a we have shown that PAPM does not exhibit mesogenic characteristics. However, in the preparation of a combined MCSCLCP from a mixture of PABP and *p*-toluenesulfonic acid (TSA) via ionic interactions, we had to first confirm that monomer PAPM is capable of forming ionic interactions when it is mixed with TSA and the mixture gives rise to a mesogenic phase. For this, we prepared a mixture of PAPM with TSA in a common solvent, ethanol. Figure 13 gives DSC thermograms for a mixture of PAPM and TSA at a scanning rate of 20 °C/min. In the inset of Figure 13 is given

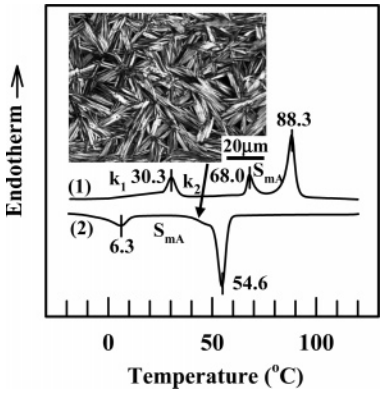

Figure 13. DSC thermograms for self-assembled PAPM-TSA at a scanning rate of 20 °C/min during (1) heating and (2) cooling cycles and POM image taken at 40 °C during the cooling cycle. Here k denotes the crystalline phase, and SmA denotes a smectic A phase.

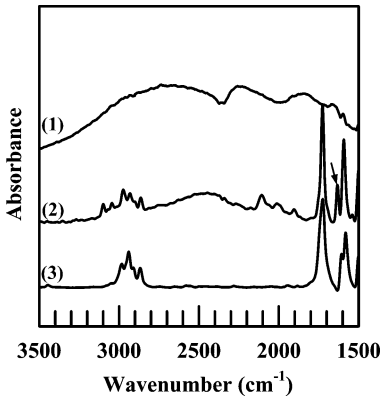

Figure 14. FTIR spectra for (1) TSA, (2) self-assembled PAPM-TSA, and (3) PAPM at room temperature.

a POM image for a mixture of PAPM and AA obtained at 40 °C during cooling, from which we observe that the mixture forms a smectic A mesophase. From the DSC thermograms in Figure 13 we observe that during heating the mixture undergoes a crystal-to-crystal (k1−k2) transition at ca. 30 °C, then a crystal-to-smectic (k2−S) transition at ca. 68 °C, and finally a S−I transition at ca. 88 °C, while during cooling the mixture undergoes an I−S transition at ca. 54 °C followed by a smectic-to-crystal transition at ca. 6 °C. Thus, we conclude that a mixture of PAPM and TSA has induced a smectic A mesophase via ionic interactions between the azopyridine group in PAPM and the sulfonic acid group in TSA.

Figure 14 gives FTIR spectra for (1) TSA, (2) a mixture of PAPM and TSA, and (3) PAPM at room temperature. It can be seen in Figure 14 that a mixture of PAPM and TSA exhibits a new absorption peak (indicated by an arrow) at a wavenumber of 1632 cm^{-1}, which is characteristic of ionized pyridyl group,[57,58] whereas the absorption peak at 1596 cm^{-1} representing the pyridyl group in the side chain of PAPM disappears. Also, the broad absorption peak from 2500 to 3000 cm^{-1} for the sulfonic acid group in TSA has become weakened, and a new absorption peak at a wavenumber of 2500 cm^{-1} is formed. The above observations have ensured us that the azopyridyl group in monomer PAPM, when it was mixed with *p*-toluenesulfonic acid (TSA), indeed formed ionic interactions, yielding a mesogenic phase.

(b) Thermal Transition and Mesophase Structure of Self-Assembled PABP−TSA. Figure 15 gives DSC thermograms for self-assembled PABP−TSA during the heating and cooling cycles at a scanning rate of 20 °C/min. It can be seen from

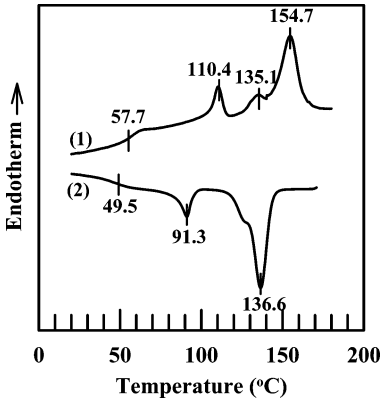

Figure 15. DSC thermograms at a scanning rate of 20 °C/min for self-assembled PABP-TSA during (1) heating and (2) cooling cycles.

Figure 15 that, upon heating, self-assembled PABP−TSA has a T_g of ca. 58 °C, a melting temperature (T_{m2}) of ca. 110 °C, and a T_{SI} of ca. 155 °C, while the phase transition temperatures during cooling are slightly decreased. The small endothermic peak appearing at 135 °C in Figure 15 is believed to have originated from the presence of high-temperature melting crystals. It has been reported[68−70] that some LCPs undergo "dual" melting processes, namely, (1) a fast melting process and (2) a slow melting process. The fast melting process is associated with the melting of usual crystallizable polymers, and the melting temperature associated with this process is usually denoted by T_{m2}. The slow melting process is associated with the melting of crystals that were formed during isothermal annealing and the temperature associated with this process is usually denoted by T_{m1}. Note that $T_{m2} < T_{m1}$, and the value of T_{m2} remains more or less constant regardless of the duration of annealing while the value of T_{m1} may increase with increasing duration of annealing.

POM images (not presented here) also indicate that self-assembled PABP−TSA has smectic mesophase structure. Referring to the DSC thermograms given in Figure 9a for PABP, we observe that PABP is a highly crystalline polymer, and it does not exhibit a glass transition over the range of temperatures investigated. The appearance of T_g in self-assembled PABP−TSA (Figure 15) indicates that the ionic interactions are much stronger than self-association within PABP molecules, and thus they restrict the mobility of molecular chains or increase the intermolecular interactions (i.e., molecular packing). Comparison of Figure 15 with Figure 9a indicates that the area under the low-temperature melting peak (T_{m2}) appearing at 110 °C for self-assembled PABP−TSA is much smaller than the area under the endothermic peak appearing at 113 °C for PABP, suggesting that the crystallinity of self-assembled PABP−TSA is very much decreased owing to the restricted mobility of molecular chains in self-assembled PABP−TSA.

(c) In Situ FTIR Spectra for Self-Assembled PABP−TSA. Figure 16 gives the FTIR spectrum for PABP taken at room temperature (denoted by *), and in situ FTIR spectra for self-assembled PABP−TSA at various temperatures, during heating, ranging from 25 to 160 °C. The following observations are worth noting in Figure 16. (1) In the inset of Figure 16, we observe a new absorption peak appearing at a wavenumber of 1632 cm^{-1} for self-assembled PABP−TSA, which is attributed to the ionic interactions between the pyridyl group in the side chain of PABP and the sulfonic acid group in TSA. The absorption peak at a wavenumber of ca. 1594 cm^{-1} for the pyridyl group has become rather weak. (2) As the temperature is increased, the strength of absorption peaks has not changed

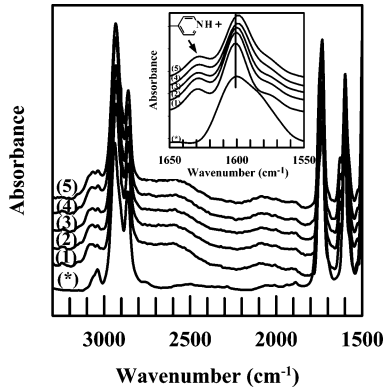

Figure 16. FTIR spectrum for PABP denoted by (*) and in situ FTIR spectra for self-assembled PABP-TSA at various temperatures (°C): (1) 25, (2) 100, (3) 120, (4) 140, and (5) 160. The inset shows the absorption peaks at wavenumbers ranging from 1650 to 1550 cm^{-1}.

much, even at temperatures close to the clearing temperature. (3) The broad absorption peak at wavenumbers ranging from 2500 to 3000 cm^{-1} for the sulfonic acid group in TSA has been weakened due to the ionic interactions with the pyridyl group in the side chain of PABP, and thus we observe a relatively weaker absorption peak at a wavenumber of 2600 cm^{-1}.

4. Concluding Remarks

In this study we synthesized three self-assembled MCSCLCPs: PyHQ12−7CNCOOH, PABP−AA, and PABP−TSA. Self-assembled PyHQ12−7CNCOOH was prepared via hydrogen bonding between the pendent pyridyl group in the MCLCP PyHQ12 and the carboxylic acid group in the mesogenic small molecule 7CNCOOH. Self-assembled PABP−AA was prepared via hydrogen bonding between the nonmesogenic side-chain azopyridyl group in the MCLCP PABP and the carboxylic acid group in the nonmesogenic small molecule *p*-anisic acid (AA). On the other hand, self-assembled PABP-TSA was prepared via ionic interactions between the nonmesogenic side-chain azopyridyl group in the MCLCP PABP and the sulfonic acid group in the nonmesogenic small molecule *p*-toluenesulfonic acid (TSA). We confirmed via FTIR spectroscopy that the hydrogen bonds or ionic interactions were formed in the respective MCSCLCPs. We found that self-assembled PyHQ12−7CNCOOH is a glassy LCP having nematic mesophase, while self-assembled PABP-AA and self-assembled PABP-TSA are semicrystalline LCPs having smectic mesophase. Interestingly, we found from in situ FTIR spectroscopy that the intermolecular hydrogen bonding between the pendent pyridyl groups in the MCLCP PyHQ12 and the carboxylic acid groups in the mesogenic small molecule 7CNCOOH and between the side-chain azopyridyl groups in the MCLCP PABP and the carboxylic acid groups in the nonmesogenic small molecule AA and the ionic interactions between the side-chain azopyridyl groups in the MCLCP PABP and the sulfonic acid group in the nonmesogenic small molecule TSA are sufficiently strong, persisting at temperatures well above the clearing temperature of the respective MCSCLCPs. This observation has enabled us to explain why, upon cooling from the isotropic state, the mesophase structure reappeared very quickly in the respective self-assembled MCSCLCPs synthesized in this study. To our knowledge, this is the first study reporting on the synthesis of combined MCSCLCP via hydrogen bonding or ionic interactions, while the previous studies[29−38] reported on the syntheses of combined MCSCLCPs were based on covalent bonding via condensation polymerization.

Acknowledgment. This study was supported in part by the National Science Foundation under Grant CST-04006752, for which we are very grateful. We acknowledge with deep gratitude that Professor Jin Kon Kim at the Department of Chemical Engineering, Pohang University of Science and Technology in the Republic of Korea, has kindly undertaken measurements of wide-angle X-ray diffraction of our samples at elevated temperatures, the results of which are reproduced in Figure 11. We gladly acknowledge very constructive comments/suggestions of an anonymous reviewer, which helped us to improve the original manuscript.

References and Notes

(1) Roviello, A.; Sirigu, A. *J. Polym. Sci., Polym. Lett. Ed.* **1975**, *13*, 455.
(2) Roviello, A.; Sirigu, A. *Eur. Polym. J.* **1979**, *15*, 61.
(3) Roviello, A.; Sirigu, A. *Eur. Polym. J.* **1979**, *15*, 423.
(4) van Luyen, D.; Strzelecki, L. *Eur. Polym. J.* **1980**, *16*, 303.
(5) Griffin, A. C.; Havens, S. *J. Polym. Sci., Polym. Phys. Ed.* **1981**, *19*, 951.
(6) Antoun, S.; Lenz, R. W.; Jin, J.-I. *J. Polym. Sci., Polym. Phys. Ed.* **1981**, *19*, 1901.
(7) Blumstein, A.; Thomas, O. *Macromolecules* **1982**, *15*, 1264.
(8) Ober, C. K.; Jin, J.-I.; Lenz, R. W. *Polym. J.* **1982**, *14*, 9.
(9) Zhou, Q.; Lenz, R. W. *J. Polym. Sci., Polym. Chem. Ed.* **1983**, *21*, 3313.
(10) Furukawa, A.; Lenz, R. W. *Macromol. Chem., Macromol. Symp.* **1986**, *2*, 3.
(11) Kricheldorf, H. R.; Domschke, A.; Schwarz, G. *Macromolecules* **1991**, *24*, 1101.
(12) Percec, V.; Yourd, R. *Macromolecules* **1989**, *22*, 3229.
(13) Percec, V.; Tsuda, Y. *Macromolecules* **1990**, *23*, 3509.
(14) Percec, V.; Zuber, M.; Ungar, G.; Alvarez-Castillo, A. *Macromolecules* **1992**, *25*, 1193.
(15) Chang, S.; Han, C. D. *Macromolecules* **1997**, *30*, 1670.
(16) Rodriguez-Parad, J. M.; Percec, V. *J. Polym. Sci., Polym. Chem. Ed.* **1986**, *24*, 1363.
(17) Komiya, Z.; Pugh, C.; Schrock, R. R. *Macromolecules* **1992**, *25*, 6586.
(18) Imrie, C. T.; Karasz, F. E.; Attard, G. S. *Macromolecules* **1992**, *25*, 1278.
(19) Komiya, Z.; Schrock, R. R. *Macromolecules* **1993**, *26*, 1393.
(20) Hsiue, G.-H.; Wen, J.-S.; Hsu, C.-S. *Polym. Bull. (Berlin)* **1993**, *30*, 141.
(21) Bohnert, R.; Finkelmann, H. *Makromol. Chem., Rapid Commun.* **1993**, *14*, 139.
(22) Laus, M.; Bignozzi, M. C.; Angeloni, A. S.; Galli, G.; Chiellini, E. *Macromolecules* **1993**, *26*, 3999.
(23) Imrie, C. T.; Karasz, F. E.; Attard, G. S. *Macromolecules* **1994**, *27*, 1578.
(24) Craig, A. A.; Imrie, C. T. *Macromolecules* **1995**, *28*, 3617.
(25) Kawakami, Y.; Toida, K. *Macromolecules* **1995**, *28*, 816.
(26) Winkler, B.; Ungerank, M.; Stelzer, F. *Macromol. Chem. Phys.* **1996**, *197*, 2343.
(27) Lin, H.-C.; Lin, Y.-S.; Lin, Y.-S.; Chen, Y.-T.; Chao, I.; Li, T.-W. *Macromolecules* **1998**, *31*, 7298.
(28) Lee, K. M.; Han, C. D. *Macromolecules* **2002**, *35*, 6263.
(29) Reck, B.; Ringsdorf, H. *Makromol. Chem., Rapid Commun.* **1985**, *6*, 291.
(30) Kapitza, H.; Zentel, R. *Makromol. Chem.* **1988**, *189*, 1793.
(31) Kapitza, H.; Zentel, R. *Makromol. Chem.* **1991**, *192*, 1839.
(32) Poths, H.; Zentel, R.; Vallerien, S. U.; Kremer, F. *Mol. Cryst. Liq. Cryst.* **1991**, *203*, 101.
(33) Zentel, R.; Brehmer, R. *Acta Polym.* **1996**, *47*, 141.
(34) Reck, B.; Ringsdorf, H. *Makromol. Chem., Rapid Commun.* **1986**, *7*, 389.
(35) Reck, B.; Ringsdorf, H.; Gardner, K.; Starkweather, H. *Makromol. Chem.* **1989**, *190*, 2511.
(36) Piao, X. L.; Kim, J.-S.; Yun, Y.-K.; Jin, J.-I. *Macromolecules* **1997**, *30*, 2294.
(37) Ge, J. J.; Zhang, A.; McCreight, K. W.; Ho, R.-M.; Wang, S.-Y.; Jin, X.; Harris, F. W.; Cheng, S. *Macromolecules* **1997**, *30*, 6498.
(38) Zhou, M.; Han, C. D. *Macromolecules* **2005**, *38*, 9602.
(39) Jeffrey, G. A. *An Introduction to Hydrogen Bonding*; Oxford University Press: New York, 1997.
(40) Kato, T.; Fréchet, J. M. *Macromolecules* **1989**, *22*, 3818.
(41) Kato, T.; Kihara, H.; Uryu, T.; Fujishima, A.; Fréchet, J. M. *Macromolecules* **1992**, *25*, 6836.
(42) Kumar, U.; Kato, T.; Fréchet, J. M. *J. Am. Chem. Soc.* **1992**, *114*, 6630.

(43) Kato, T.; Fréchet, J. M. *Macromol. Symp.* **1993**, *98*, 311.
(44) Kato, T.; Kihara, H.; Kumar, U.; Uryu, T.; Fréchet, J. M. *Angew. Chem., Int. Ed. Engl.* **1994**, *33*, 1644.
(45) Kato, T.; Ihata, O.; Ujiie, S.; Tokita, M.; Watanabe, J. *Macromolecules* **1999**, *31*, 3551.
(46) Ihata, O.; Yokota, H.; Kanie, K.; Ujiie, S.; Kato, T. *Liq. Cryst.* **2000**, *27*, 69.
(47) Cui, L.; Zhao, Y. *Chem. Mater.* **2004**, *16*, 2076.
(48) Alexander, C.; Jariwala, C. P.; Griffin, A. C. *Polymer* **1994**, *35*, 4550.
(49) Alexander, C.; Jariwala, C. P.; Griffin, A. C. *Macromol. Symp.* **1994**, *77*, 283.
(50) Lee, C.-M.; Griffin, A. C. *Macromol. Symp.* **1997**, *117*, 281.
(51) Malik, S.; Dhal, P. K.; Mashelkar, R. A. *Macromolecules* **1995**, *28*, 2159.
(52) Lehn, J. M. *Angew. Chem., Int. Ed. Engl.* **1990**, *29*, 1304.
(53) Paleos, C. M.; Tsiourvas, D. *Liq. Cryst.* **2001**, *28*, 1127.
(54) Eisenberg, A.; Smith, P. *Polym. Eng. Sci.* **1982**, *22*, 1117.
(55) Smith, P.; Eisenberg, A. *J. Polym. Sci., Polym. Lett. Ed.* **1983**, *21*, 223.
(56) Rutkowska, M.; Eisenberg, A. *Macromolecules* **1984**, *17*, 821.
(57) Chen, W.; Sauer, J. A.; Hara, M. *Polymer* **2003**, *44*, 7729.
(58) Chen, W.; Sauer, J. A.; Hara, M. *Polymer* **2004**, *45*, 7219.
(59) Vuillaume, P. Y.; Bazuin, C. G. *Macromolecules* **2003**, *36*, 6378.
(60) Faul, C. F. J.; Antonietti, M. *Adv. Mater.* **2003**, *15*, 673.
(61) Guan, Y.; Yu, S.-H.; Antonietti, M.; Böttcher, C.; Faul, C. F. J. *Chem.—Eur. J.* **2005**, *11*, 1305.
(62) Kim, S. S.; Han, C. D. *Polymer* **1994**, *35*, 93.
(63) Sato, A.; Kato, T.; Uryu, T. *J. Polym. Sci., Polym. Chem. Ed.* **1996**, *34*, 503.
(64) Lee, K. M.; Han, C. D. *Macromolecules* **2002**, *35*, 3145.
(65) Coleman, M. M.; Graff, J. F.; Painter, P. C. *Specific Interactions and the Miscibility of Polymer Blends*; Technomic Publishing: Lancaster, PA, 1991.
(66) Hsu, C.-S.; Lin, J.-H.; Chou, L.-R.; Hsiue, G.-H. *Macromolecules* **1992**, *26*, 7126.
(67) Felekis, T.; Tziveleka, L.; Tsiourvas, D.; Paleos, C. M. *Macromolecules* **2005**, *38*, 1705.
(68) Lin, Y. G.; Winter, H. H. *Macromolecules* **1988**, *21*, 2439.
(69) Cheng, S. Z. D.; Zhang, A.; Johnson, R. L. Wu, Z.; Wu, H. H. *Macromolecules* **1990**, *23*, 1196.
(70) Nam, J.; Fukai, T.; Kyu, T. *Macromolecules* **1991**, *24*, 6250.
(71) Kim. S. S.; Han, C. D. *Macromolecules* **1993**, *26*, 3176.

MA052716Q